A PLANE-WAVE BASED SEISMIC INTERFEROMETRY FOR CONTROLLED-SOURCE DATA

Yi Tao and Mrinal K. Sen

Jackson School of Geological Sciences
The University of Texas at Austin

ABSTRACT

We present a new approach to retrieve virtual seismic responses from crosscorrelating controlled-source seismic data in the plane-wave domain. This method is based on slant stacking over shot or receiver locations of observed seismic data to produce plane-wave transformed gathers. Crosscorrelation is then performed by selecting the same ray parameters from different shot or receiver locations. Unlike a traditional approach where the correlogram is obtained from crosscorrelating recorded data which contains the full range of ray parameters, this method directly chooses common ray parameters to cancel overlapping ray paths. Thus, it can sometime avoid spurious arrivals when the acquisition requirement of seismic interferometry is not strictly met with. In addition, in the plane-wave domain, we can choose certain range of ray parameters so that we can retrieve energy only from certain directions. This method can also help to save computation time because plane-wave transformed data usually results in a reduction of the original data volume. We demonstrate our method with synthetic and an OBS data examples.

INTRODUCTION

In recent years, seismic interferometry, also known as Green's function retrieval, has grown to be a thriving research area with many novel applications. Because it can redatum the seismic data from the acquisition geometry to another source or receiver related geometry, and because this redatuming does not require a velocity model, this technique has been applied extensively to controlled-source exploration data (e.g., Schuster 2001, Wapenaar 2006, Bakulin and Calvert 2006, Curtis et al., 2009). Another major type of data where seismic interferometry has been widely applied is passive seismic data with natural sources (e.g., Rickett and Claerbout 1999, Shapiro et al., 2005, Draganov et al., 2007). For a comprehensive review of the theory and applications of seismic interferometry, the reader is referred to Schuster (2009), and Wapenaar et al. (2010a and 2010b).

In classical interferometry, a virtual trace is obtained by crosscorrelating at two different receiver or source locations. Under high-frequency approximation, this process can be viewed as cancelation of common part of a ray path from a physical source to the two different receivers. This cancelation results in a raypath between the virtual source and a receiver (Schuster et al.,

2004). A stacking operator is then applied to the correlogram to take advantage of contributions of all the sources. This entire process is done in the time-space ($t-\mathbf{x}$) domain or in its equivalent frequency domain. However, in this domain, sources and receivers may be irregularly positioned and if a large number of traces need to be crosscorrelated, it can be computationally time consuming, especially when the crosscorrelation is done in time domain.

Transforming seismic data from time-space domain to the plane-wave ($\tau-\mathbf{p}$) domain involves a mapping from original source and receiver distributions to ray parameter ($\mathbf{p}$) distributions (e.g., Stoffa et al., 2006). It results in a regularized coordinate system even for irregular input data. This mapping is generally applicable to controlled-source data, such as surface seismic profile (SSP) and vertical seismic profile (VSP), both of which are typically considered in seismic interferometry (Schuster and Zhou, 2006). This mapping is also applicable to refraction geometry used in a recent work of super-virtual interferometry (Mallison et al., 2011). In the plane-wave domain, each ray parameter corresponds to a certain angle of incident seismic waves. This transformation offers several advantages and numerous methods have been investigated for seismic wave filtering (Tatham 1989), multiple attenuation (Liu et al., 2000), seismic forward modeling (Vigh and Starr 2008), migration (Stoffa et al., 2006) and inversion (Sen et al., 2003).

In this paper, we propose retrieving seismic responses based on crosscorrelation in the plane-wave domain. Classical interferometry automatically finds a ray from a stationary source, passing through two different receivers and cancels the common ray path. Plane-wave domain interferometry decomposes the data into different ray parameters and cancels the common ray paths by crosscorrelating the same ray parameters. We will demonstrate that this method can obtain results similar to those obtained in time-space domain, but it offers several advantages such as a regular coordinate system, computational efficiency and the flexibility to choose ray parameters for seismic data redatuming.

THEORY

Plane-wave transform

Plane-wave transform, also known as $\tau-\mathbf{p}$ transform or slant stack, has been investigated by many authors (e.g. Stoffa et al., 1989, Foster and Mosher 1992). The key idea of this transformation is to obtain "ray-parameter" gathers from common shot or common receiver gathers. It can be implemented either in time domain or in frequency domain. In the time domain, it involves summing of amplitudes along lines of constant slope called ray-parameters. In the frequency domain, this transform involves a phase shift determined by ray parameters and offsets and a summation over offsets. For acquisition geometries with surface sources and

surface receivers or for transmission problems, the frequency domain version of plane-wave transform can be written as follows

$$\tilde{d}(\mathbf{p}\,|\,\mathbf{x},\omega) = \int d(\mathbf{h}\,|\,\mathbf{x},\omega)\exp(i\omega\mathbf{ph})d\mathbf{h}. \tag{1}$$

where $d(\mathbf{h}\,|\,\mathbf{x},\omega)$ is the recorded data in the frequency domain, $\mathbf{h}$ is offset and $\mathbf{h} = \mathbf{x_r} - \mathbf{x_s}$, $\mathbf{x}$ is the receiver position for a shot gather and it is the source position for a receiver gather, $\tilde{d}(\mathbf{p}\,|\,\mathbf{x},\omega)$ is the transformed plane-wave gather for a certain offset. The inverse plane-wave transform can be defined as

$$\tilde{d}(\mathbf{p_r}\,|\,\mathbf{x_s},\omega) = \int d(\mathbf{x_r}\,|\,\mathbf{x_s},\omega)\exp(i\omega\mathbf{p_r}\mathbf{x_r})d\mathbf{x_r}. \tag{2}$$

For the interferometric problem considered here, using the plane-wave transform related to absolute receiver position $\mathbf{x_r}$ or absolute source position $\mathbf{x_s}$ is more helpful. The forward and inverse transform for a shot gather are given by

$$\tilde{d}(\mathbf{p_r}\,|\,\mathbf{x_s},\omega) = \int d(\mathbf{x_r}\,|\,\mathbf{x_s},\omega)\exp(i\omega\mathbf{p_r}\mathbf{x_r})d\mathbf{x_r}. \tag{3}$$

$$d(\mathbf{x_r}\,|\,\mathbf{x_s},\omega) = \omega^2 \int \tilde{d}(\mathbf{p_r}\,|\,\mathbf{x_s},\omega)\exp(-i\omega\mathbf{p_r}\mathbf{x_r})d\mathbf{p_r}. \tag{4}$$

where $d(\mathbf{x_r}\,|\,\mathbf{x_s},\omega)$ is a shot record with source coordinate $\mathbf{x_s}$ and receiver coordinate $\mathbf{x_r}$. Similarly, for receiver gather, we can use the following formulas

$$\tilde{d}(\mathbf{P_s}\,|\,\mathbf{x_r},\omega) = \int d(\mathbf{x_s}\,|\,\mathbf{x_r},\omega)\exp(i\omega\mathbf{P_s}\mathbf{x_s})d\mathbf{x_s}. \tag{5}$$

$$d(\mathbf{x_s}\,|\,\mathbf{x_r},\omega) = \omega^2 \int \tilde{d}(\mathbf{P_s}\,|\,\mathbf{x_r},\omega)\exp(-i\omega\mathbf{P_s}\mathbf{x_s})d\mathbf{P_s}. \tag{6}$$

Seismic response retrieval in the plane-wave domain

A general representation of the Green's function retrieval process between two positions is based on the Rayleigh reciprocity theorem (Wapenaar 2004, Schuster 2009). In this paper we use a far-field approximation and ignore the absolute amplitude. The retrieval of seismic response using interferometry relation in the frequency domain can be written as (e.g., Wapenaar et al. 2010a)

$$\begin{aligned} d(\mathbf{x_B}\,|\,\mathbf{x_A},\omega) + d^*(\mathbf{x_B}\,|\,\mathbf{x_A},\omega) &\approx \\ \int d^*(\mathbf{x_A}\,|\,\mathbf{x},\omega)d(\mathbf{x_B}\,|\,\mathbf{x},\omega)d\mathbf{x} \end{aligned} \tag{7}$$

where $d^*(\mathbf{x_A}\,|\,\mathbf{x_B},\omega)$ represents the complex conjugate seismic wavefield with $\mathbf{x_B}$ is the source coordinate and $\mathbf{x_A}$ is the receiver coordinate.

Using equation 3 or equation 5, decomposition of seismic wavefield $d(\mathbf{x_A} \mid \mathbf{x_B}, \omega)$ into frequency-ray parameter ($\omega - \mathbf{p}$) domain can be accomplished by summing the data over all the $\mathbf{x}$ positions

$$\tilde{d}(\mathbf{p_A} \mid \mathbf{x}, \omega) = \int d(\mathbf{x_A} \mid \mathbf{x}, \omega) \exp(i\omega \mathbf{p_A} \mathbf{x}) d\mathbf{x}. \tag{8}$$

where $\mathbf{p_A}$ represents a ray parameter related to survey position $\mathbf{x_A}$. Similar to equation 4 or 6, the inverse transform is defined as

$$d(\mathbf{x_A} \mid \mathbf{x}, \omega) = \omega^2 \int \tilde{d}(\mathbf{p_A} \mid \mathbf{x}, \omega) \exp(-i\omega \mathbf{p_A} \mathbf{x}) d\mathbf{p_A} \tag{9}$$

We can also define a plane-wave transform by summing over all offsets, but here we need the absolute survey positions to derive interferometric relations in the plane-wave domain. After this transform, the complex conjugate wavefield $d(\mathbf{x_A} \mid \mathbf{s}, \omega)$ in the frequency domain is given by

$$d^*(\mathbf{x_A} \mid \mathbf{x}, \omega) = \omega^2 \int \tilde{d}^*(\mathbf{p_A} \mid \mathbf{x}, \omega) \exp(i\omega \mathbf{p_A} \mathbf{x}) d\mathbf{p_A}. \tag{10}$$

Inserting equation 10 into equation 7, we obtain

$$\begin{aligned} d(\mathbf{x_B} \mid \mathbf{x_A}, \omega) &+ d^*(\mathbf{x_B} \mid \mathbf{x_A}, \omega) \\ &\approx \omega^2 \int\int \tilde{d}^*(\mathbf{p_A} \mid \mathbf{x}, \omega) d(\mathbf{x_B} \mid \mathbf{x}, \omega) \exp(i\omega \mathbf{p_A} \mathbf{x}) d\mathbf{x} d\mathbf{p_A} \end{aligned} \tag{11}$$

Notice that though $\mathbf{p_A}$ and $\mathbf{p_B}$ relate to different positions, they can be of the same value if we choose the range and step of the ray parameters to be the same. Thus,

$$\begin{aligned} d(\mathbf{x_B} \mid \mathbf{x_A}, \omega) &+ d^*(\mathbf{x_B} \mid \mathbf{x_A}, \omega) \\ &\approx \omega^2 \int\int \tilde{d}^*(\mathbf{p_A} \mid \mathbf{x}, \omega) d(\mathbf{x_B} \mid \mathbf{x}, \omega) \exp(i\omega \mathbf{p_B} \mathbf{x}) d\mathbf{x} d\mathbf{p_B} \\ &= \omega^2 \int \tilde{d}^*(\mathbf{p_A} \mid \mathbf{x}, \omega) \tilde{d}(\mathbf{p_B} \mid \mathbf{x}, \omega) d\mathbf{p} \end{aligned} \tag{12}$$

When the absolute amplitude is not taken into account, the ω^2 filter ($\partial^2 / \partial t^2$ in the time domain) in the right-hand side can be considered as processing filtering effects and can be ignored (Claerbout, 1985). However, this filter is necessary to match the frequency spectrum of the original data. Thus, equation 12 in the $\tau - \mathbf{p}$ domain is equivalent to

$$\begin{aligned} d(\mathbf{x_B} \mid \mathbf{x_A}, t) &+ d^*(\mathbf{x_B} \mid \mathbf{x_A}, t) \\ &\approx \frac{\partial^2}{\partial t^2} * \int \tilde{d}^*(\mathbf{p_A} \mid \mathbf{x}, t) \otimes \tilde{d}(\mathbf{p_B} \mid \mathbf{x}, t) d\mathbf{p} \end{aligned} \tag{13}$$

where $\otimes$ denotes crosscorrelation.

Equation (6) suggests that analogous to $t-\mathbf{x}$ domain, seismic interferometry can be performed in the $\tau-\mathbf{p}$ domain by crosscorrelating two $\mathbf{p}$ traces which have the same value but are from different positions. Following a procedure of summing over all $\mathbf{p}$ traces, this will produce a virtual trace between the two points.

Suppose the input seismic data is a common shot gather. The steps to perform seismic interferometry in the tau-p domain can be described as follows

1. Input t-x domain shot gathers and sort them into common receiver gathers $d(t,\mathbf{r},\mathbf{s})$.

2. Transform the time-space domain data $d(t,\mathbf{r},\mathbf{s})$ into plane wave data $d(\tau,\mathbf{r},\mathbf{p})$ using equation 8.

3. Select master trace A and slave trace B based on the fixed receiver position A and B. Then decide the range of $\mathbf{p}$ values to perform crosscorrelation and sum over all $\mathbf{p}$ values. And then apply a ω^2 filter of the data if necessary. This results in a virtual seismic data that looks like A is the virtual source and B is the virtual receiver.

4. Loop step 3 over all the receivers and output redatumed seismic data for further processing, e.g. migration.

Plane wave interferometry can be understood by considering a simple example (Figure 1). Inteferometric redatuming in the $t-\mathbf{x}$ domain can be explained by cancelation of overlapping stationary ray paths recorded at different receivers. The Green's function between receiver B and A is retrieved by crosscorrelating a ray from source S with cancelation of the common path. In the plane-wave domain, it may be more physically acceptable using asymptotic ray explanations. There are several raypaths from source S to receiver B and A with many ray parameters; stationary condition in interferometry suggests that only those that have the same source ray parameter can lead to cancelation of overlapping ray paths (e.g., Schuster 2009). Thus, interferometry in the plane-wave domain is conducted by selecting the same source ray parameters from receiver B and A for crosscorrelation. Simply put, interferometry in the $t-\mathbf{x}$ domain is to find common path automatically from source-receiver geometry; in the plane-wave domain common path is selected by the same ray parameter.
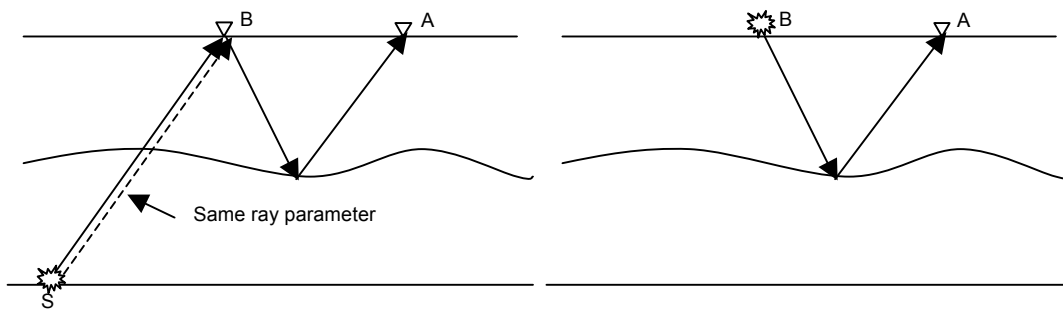

Figure 1. Crosscorrelating traces recorded at receiver locations B and A produces a new trace with virtual source at B, receiver at A. The canceled overlapping raypaths in the plane-wave domain corresponds to same ray parameters.

EXAMPLES

Example 1: Transmission to reflection retrieval

Our first example is a transmission to reflection retrieval example. The 2D acoustic subsurface model is shown in Figure 2 (modified from Draganov et al., 2006). This model consists of an irregular sea floor and a dipping layer. 600 transient sources are located at $z = 2.0$ km with an equal distance of 10m; 600 receivers are laterally positioned at the surface. After redatuming, we will get virtual surface acquisitioned marine data with both sources and receivers on the surface for this geometry.

Original shot gathers are obtained numerically by 2-D finite difference with absorbing boundary conditions. They are then sorted into common receiver gathers. The $\tau - \mathbf{p}$ transformed data using equation 2 for the first receiver gather (located at (0,0)) is shown in Figure 3 (right). The ray parameters range from -0.6 s/km to 0.6 s/km. Full wave information from $t - \mathbf{x}$ gather (Figure 3 left) is contained in this transformed gather. Interferometry is then performed over the $\tau - \mathbf{p}$ gather using step 3 and step 4.

An example crosscorrelogram of this model is shown in Figure 4. For $t - \mathbf{x}$ domain interferometry, this is obtained by first selecting a master trace with receiver located at (3km, 0) for the first subfurcace source and a slave trace with source and receiver at the same location, and then correcorrelating (autocorrelating) these two traces. This procedure is repeated for all 600 sources to produce 600 correlation traces. For plane-wave interferometry, this is obtained simply by selecting the same ray paramter from $\tau - \mathbf{p}$ transformed common receiver gather, autocorrelating it and then repeating for another ray parameter. While all 600 sources for $t - \mathbf{x}$ domain interferometry needed to correlate to produce the correlation panel (Figure 4 left), for $\tau - \mathbf{p}$ domain interferometry (Figure 4 right), we can observe that most of the energy are produced in a certain range of ray parameters (about -0.3 s/km to 0.3 s/km for this case). This range corresponds to the stationary-phase region (Draganov et al., 2006). Also, note that the range of ray parameters in the correlation panel is smaller than the range of ray parameters in the receiver gather (about -0.5 s/km to 0.5 s/km).

Stacking of the crosscorrelogram in Figure 4 results in a reconstructed trace with source and receiver at the same surface location (3km, 0). From crosscorrelogram, we can observe that with $\tau - \mathbf{p}$ domain interferometry, there is some diffracted energy at the edge of the panel because of the finite aperture of seismic acquisition. This is because in reality, ideal interferometric geometries which require that the medium be completely surrouned by physical sources (Wapenaar 2004), are never satisfied. After stacking, these diffractions cancel out and the zero-offset trace using $\tau - \mathbf{p}$ domain interferometry and t-x domain interferometry produce nearly identical results, both in travel time and normalized amplitude (Figure 5).

Figures 6a and 6b show the retrieved surface reflection data for one virtual shot gather using interferometry in these two different domains. The virtual source is located at (3km, 0) and virtual receivers are located along the surface so that we can see the symmetric two-sided seismic response. The two plots are generated using the same gain. There are no noticeable

differences between the two except for the absolute amplitude. This suggests when the distribution of sources and receivers is satisfied for interferometric redatuming, time-space domain interferometry and plane-wave domain interferometry should produce similar results. When the acquisition condition is satisfied, correlating the data using all available ray information at one receiver location with another receiver location (time-space domain) should give similar result as correlating data that has the same ray parameter (plane-wave domain approach).

When seismic data do not have adequate spatial sampling and sufficient acquisition aperture, $\tau-p$ transform is known to suffer from edge effects and numerical aliasing. However, seismic interferometry requires a range of ray parameters and when stacked together, such artifacts are not noticeable (Figure 6 (c) and (d)).
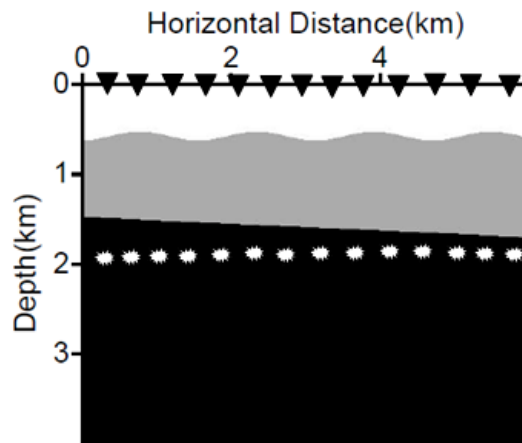
Figure 2. An acoustic velocity structure for transmission to reflection retrieval for marine data. This model has a water layer with velocity=1.5 km/s, an irregular sea floor followed by a layer with velocity=2.0 km/s, velocity after the dipping layer is 3.0 km/s.
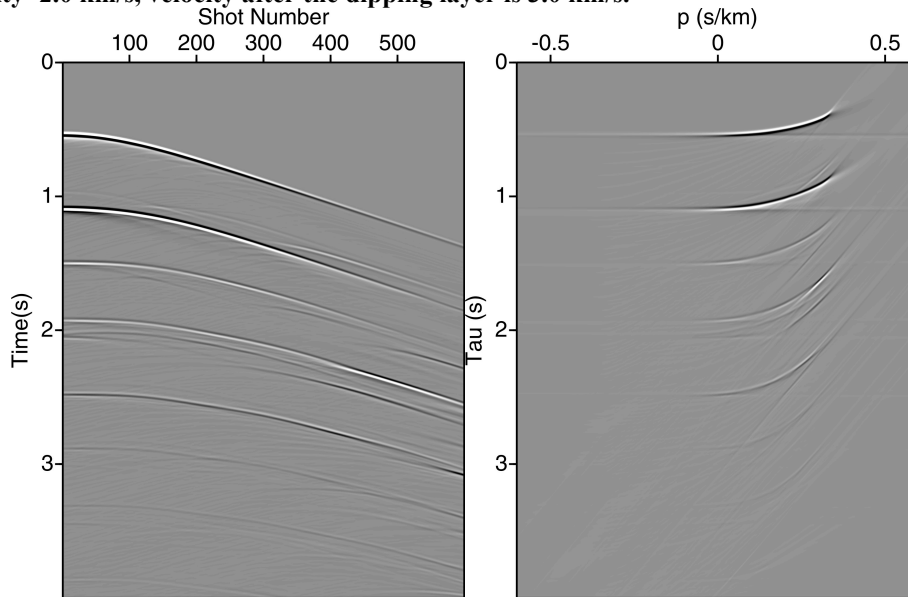
Figure 3. Common receiver gather for the first receiver (left) and its tau-p transformed gather (right). There are 200 ray parameters in the plane-wave gather from -0.6 to 0.6 s/km.
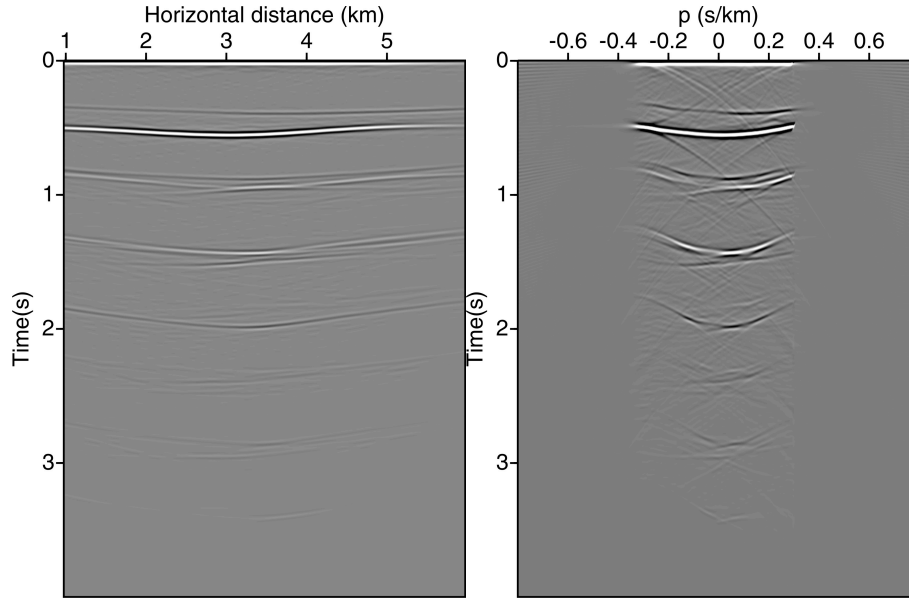
Figure 4. The crosscorrelogram for a master trace recorded at (3km,0) with a slave trace recorded at the same location for each subsurface position (only positive time is shown). Left: with time-space domain interferometry. Right: with plane-wave domain interferometry.

When seismic data do not have adequate spatial sampling and sufficient acquisition aperture, $\tau-p$ transform is known to suffer from edge effects and numerical aliasing. However, seismic interferometry requires a range of ray parameters and when stacked together, such artifacts are not noticeable (Figure 6 (c) and (d)).
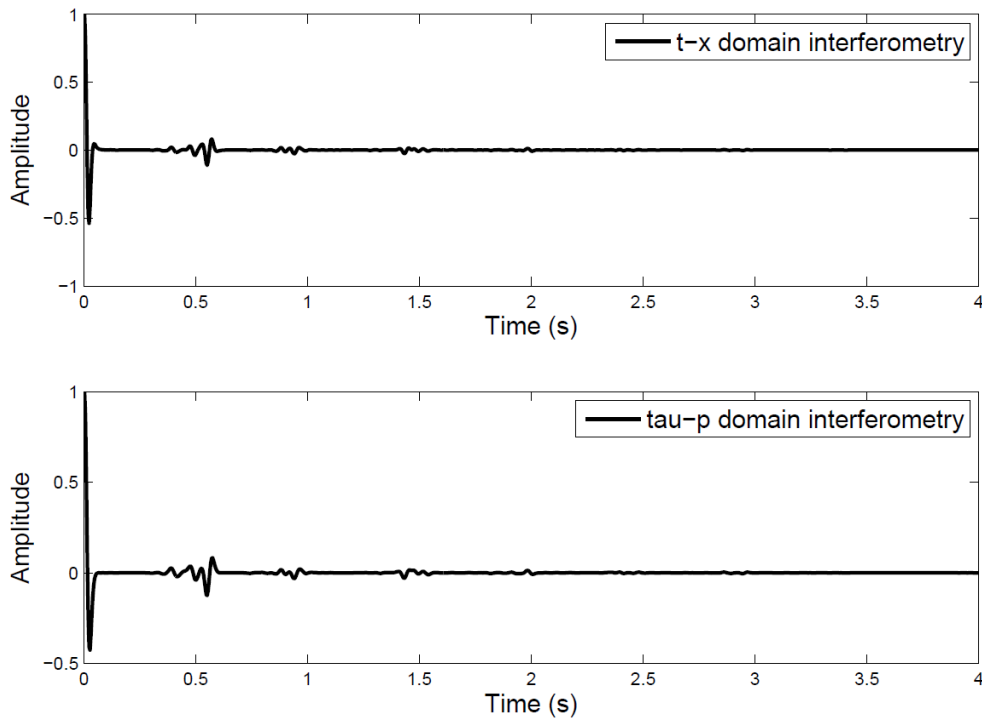
Figure 5. The summation of crosscorrelogram in Figure (4) to produce a virtual zero-offset event with source and receiver located at (3km,0). Up: with time-space domain interferometry. Bottom: with plane-wave domain interferometry.
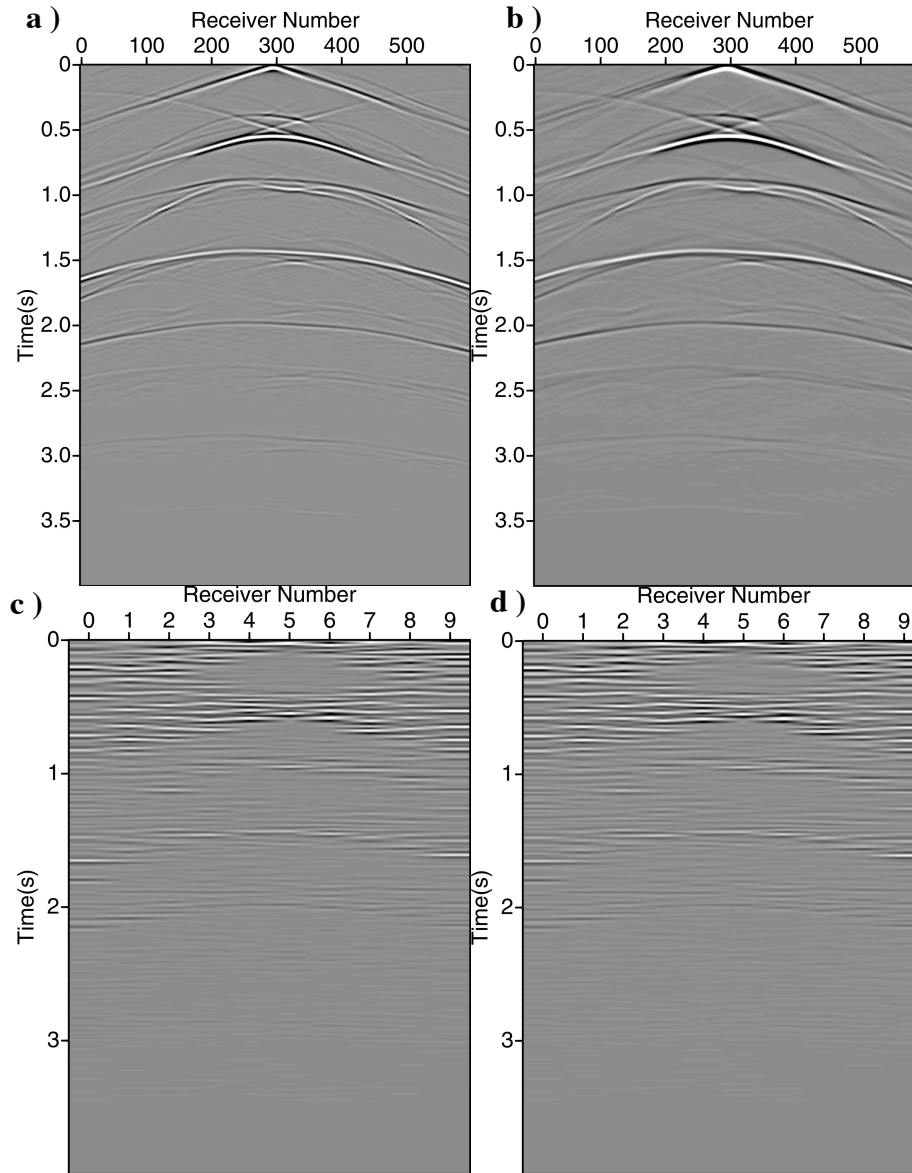
Figure 6. (a) Redatumed shot record using time-space domain interferometry for a virtual source located at (3km, 0) and receivers along the surface. (b) redatumed shot record using plane-wave domain interferometry. (c) redatumed shot record using time-space domain interferometry for only 10 real transient sources and 10 real receivers. (d) redatumed shot record using plane-wave domain interferometry. (c) and (d) has the same geometry as (a) and (b), except that the data is sparsely sampled.

One particular use of plane-wave domain interferometry is to select the range of ray parameters which has the most dominant energy. This is useful when the recorded seismic data consist of significant amount of noise, e.g., random noise and surface-wave noise in land data. These noises should be suppressed because they might contribute to spurious arrivals in the redatumed events. Similar idea of retrieving seismic data using only dominant energy was also proposed by Vidal et al., (2011). However, their approach is based on the plane-wave transform of the virtual-source panel, which differs from our approach that based on direct transform of the recorded data.
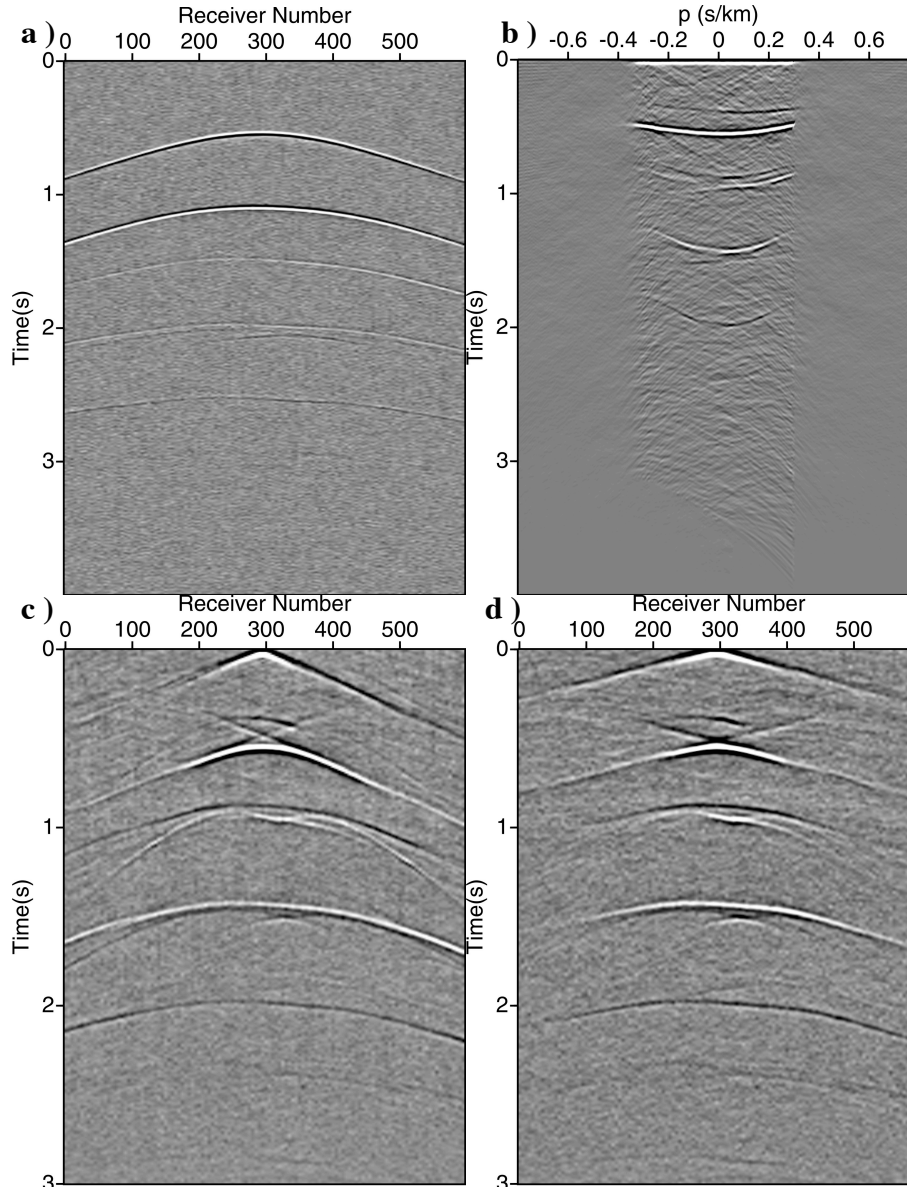
Figure 7. (a) Synthetic noisy real shot gather. (b) crosscorrelogram in the plane-wave domain. (c) redatumed virtual shot gather using full range of ray parameters. (d) redatumed virtual shot gather using only ray parameters between -0.2 s/km and 0.2 s/km.

We demonstrate this approach by simply adding random noise to the original recorded data. The synthetic shot gather is shown in Figure 7a. By analyzing the correlogram in the plane-wave domain (Figure 7b), we can observe that most of the domained ray parameters are between -0.2 s/km to 0.2 s/km. Figure 7c shows the redatumed result using full range of ray parameters. This retrieval results in reflections and diffractions. While for this case the diffraction arrivals are true in the real modeled gather, in reality, we may beinterested in retrieving reflections only. Figure 7d shows the results using range-selected ray parameters. Reflections are correctly retrieved while the diffractions are suppressed.

Example 2: VSP redatuming

We demonstrate this approach by simply adding random noise to the original recorded data. The synthetic shot gather is shown in Figure 7a. By analyzing the correlogram in the plane-wave domain (Figure 7b), we can observe that most dominant ray parameters are between -0.2 s/km to 0.2 s/km. Figure 7c shows the redatumed result using full range of ray parameters. This retrieval results in reflections and diffractions. While for this case the diffraction arrivals are true in the real modeled gather, in reality, we may beinterested in retrieving reflections only. Figure 7d shows the results using range-selected ray parameters. Reflections are correctly retrieved while the diffractions are suppressed.

Another successful application of seismic interferometry is to redatum VSP data to SSP data or Single Well Profile (SWP) data (Schuster 2009). For depth sampled data, $\tau - \mathbf{p}$ transform can be used to map the data $d(t,z)$ from time-depth domain to the plane-wave domain similar to surface seismic data. The forward and inverse transform can be defined as:

$$\tilde{d}(\mathbf{p},\omega) = \int d(z,\omega)\exp(i\omega\mathbf{p}z)dz \,. \tag{14}$$

$$d(z,\omega) = \omega^2 \int \tilde{d}(\mathbf{p},\omega)\exp(-i\omega\mathbf{p}z)d\mathbf{p} \,. \tag{15}$$

Using this transform, seismic interferometry can be performed in the plane-wave domain without any further assumptions to redatum the VSP data to either SSP or SWP data. Here we use a 2-D synthetic model (Figure 8) modified from Lu et al.,(2008) to redatum walk-away VSP data to SWP data (borehole sources and borehole receivers). For simplicity, we remove background velocity gradient of the original velocity profile and use a constant background velocity instead. The objective here is to image the synthetic salt dome with velocity similar to Gulf of Mexico salt domes.
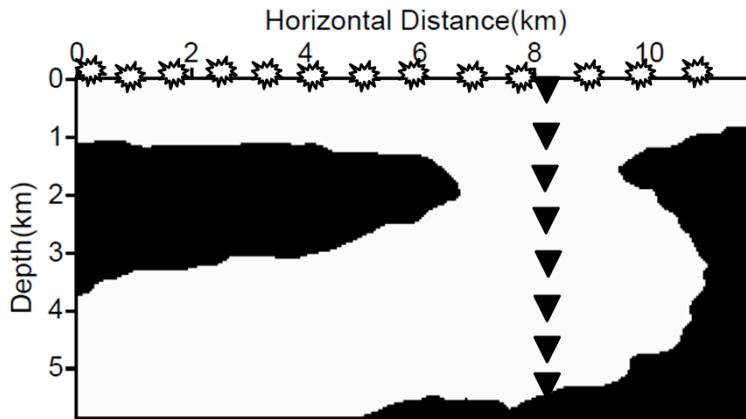

Figure 8. Walk-away VSP acquisition geometry for a synthetic test. The model is comprised of a background velocity of 2000 m/s with two salt bodies of velocity 4480 m/s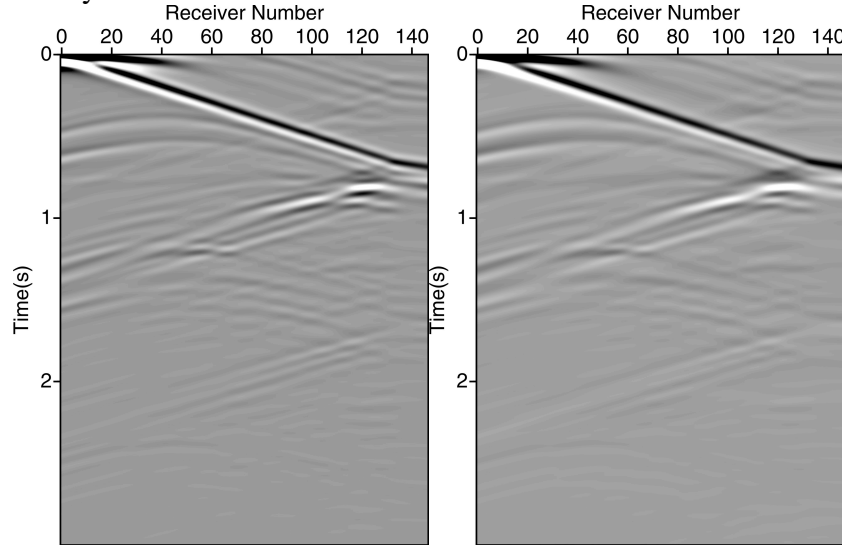. Comparion of redatumed downhole common shot gather using time-space domain interferometry (left) and in plane-wave domain interferometry (right) for a virtual source located at the surface and receivers in the borehole.

Figure 9 compares retrieved SWP data using time-space domain interferometry and plane-wave domain interferometry with $\mathbf{p}$ values ranging from -0.6 s/km to 0.6 s/km. We can observe that despite some filtering effects present in the $\tau - \mathbf{p}$ domain approach, these two methods in general produce nearly identical results.

Figure 9. Comparison of redatumed downhole common shot gather using time-space domain interferometry (left) and in plane-wave domain interferometry (right) for a virtual source located at the surface and receivers in the borehole.

Another application of $\tau - \mathbf{p}$ domain interferometry for VSP geometry is to separate left and right propagating waves using positive and negative ray parameters. Wavefield seperation has already been used in seismic interferometry with up-down separation (Mehta et al., 2007). For VSP geometry in Figure 6, if we want to image the salt dome on the right of the model, then most of the stationary-phase points are contribution by negative (or positive depending on definition) $\mathbf{p}$ values. For the model in Figure 10, redatuming using full wave represents all the reflected data from the whole subsurface geology. Waves coming from different parts of the model could intertwine with each other, and correspondingly affect the migrated image. With interferometry in the plane-wave domain, we can easily select only interested ray parameters to produce directional redatuming.
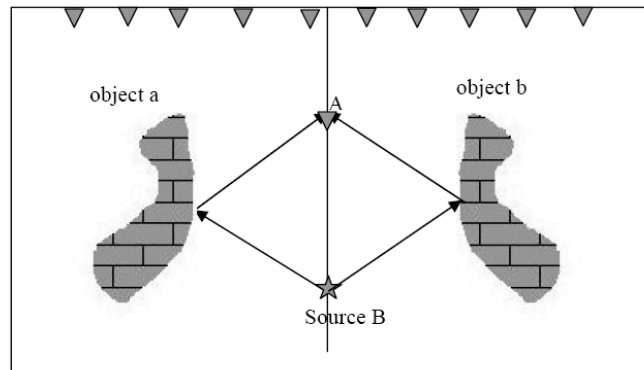

Figure 10. A model shows the limitation of conventional interferometry. There are different ray paths from A to B, can be either from the left object a or the right object b. If we migrate this data, we could not effectively delineate both of the two objects.

12

Figure 11 (left) compares redatumed shot gather using only negative **p** values, the result is similar to that using entire range of **p** values and is also similar to the result obtained by directly putting a source and receivers in the borehole (Figure 11 right). After redatuming, we performed Kirchhoff depth migration to the SWP data. The migration results with only negative ray parameters and full range of ray parameters are shown in Figure 12 left and Figure 12 right, repectively. Both of these approaches could capture the edge of the salt dome correctly. We cannot observe many differences for this model, suggesting that we can effectively delineate the salt body with only partial ray parameters. Also, migration with only negative ray parameters might get slightly better image, e.g., it can suppress some high anomlies at the location (4.8km, 0.6km) in this model.
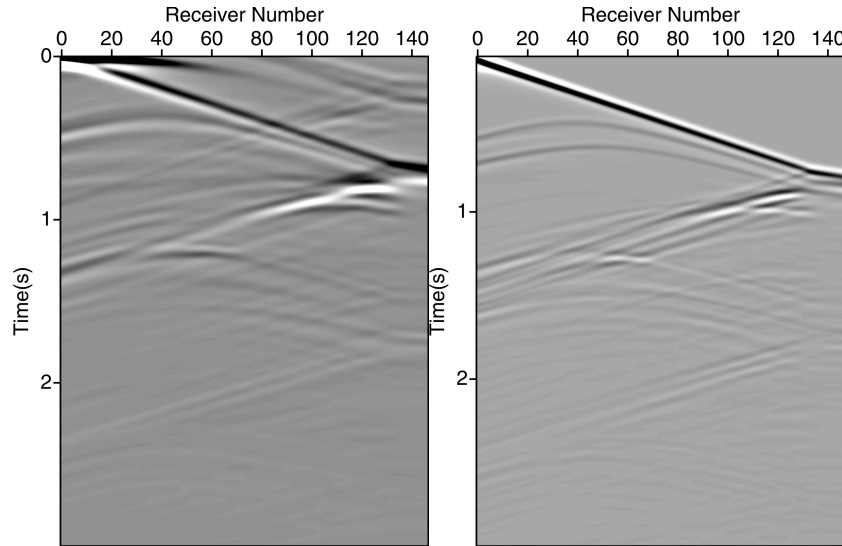

Figure 11. Comparison of plane-wave domain interferometric redatumed using only negative ray parameters ($-0.6 \, \text{s/km} < \mathbf{p} < 0$) (left) and directly putting source at surface and receivers in the borehole (right).
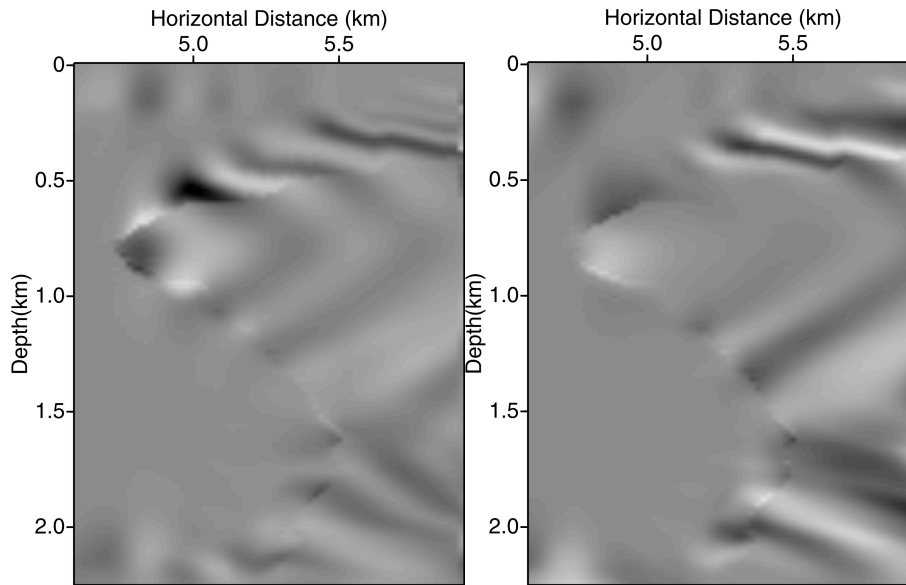

Figure 12. Comparion of depth migrated redatumed data using only negative ray parameters (left) and using full range of ray parameters (right).

Example 3: Super-virtual interferometry

Super-virtual interferometry is a novel technique to increase the signal-to-noise ratio (SNR) of far-offset refracted waves (Bharadwaj et al., 2011). With this technique, the receiver spread of the refraction survey can be fully utilized if we are only interested in the travel time information. Virtual far-offset refraction arrivals are generated by first a crosscorrelation between adjacent refracted wave traces and summation to produce a virtual trace, and then by a convolution with the actual refraction traces. Mathematically, without retrieving the absolute amplitude, these two steps can be written as follows

$$\psi(\mathbf{A}\,|\,\mathbf{B},t)^{virt} \approx \int_{source} \psi^{*}(\mathbf{X_A}\,|\,\mathbf{x},t) \otimes \psi(\mathbf{X_B}\,|\,\mathbf{x},t)d\mathbf{x}. \tag{16}$$

$$\psi(\mathbf{B}\,|\,\mathbf{A},t)^{super} \approx \int_{receiver} \psi(\mathbf{B}\,|\,\mathbf{x}',t)^{virt} \otimes \psi(\mathbf{A}\,|\,\mathbf{x}',t)d\mathbf{x}'. \tag{17}$$

where $\psi(\mathbf{A}\,|\,\mathbf{B},t)$ denotes the head wave contribution in the recorded data $d(\mathbf{A}\,|\,\mathbf{B},t)$, $\psi(\mathbf{B}\,|\,\mathbf{A},t)^{virt}$ is the virtual data by stacking the common receiver pair gather (CPG) (Dong et al., 2006), $\psi(\mathbf{B}\,|\,\mathbf{A},t)^{super}$ is the processed super-virtual head wave data. Note that the above relation works both for P-wave and shear wave.
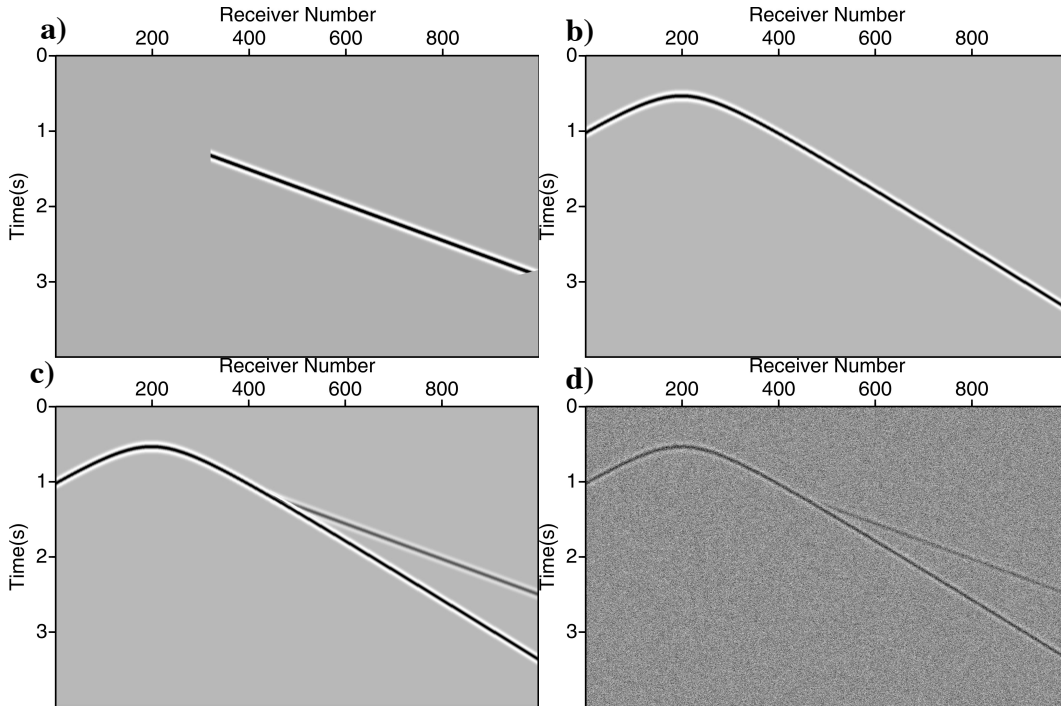

Figure 13. (a) Synthetic head wave. (b) synthetic reflection. (c) synthetic reflection plus head wave with head wave has a smaller amplitude. (d) similar to (c), but random noise is added.

Virtual traces in the CPG gather are useful to distinguish between head wave and diving wave. This is because head wave corresponds to flat events while for diving wave it is not flat.

Equation 16 has a similar formula as conventional interferometry relation (equation 7). Thus, the plane-wave domain approach is applicable to generate the CPG gather.
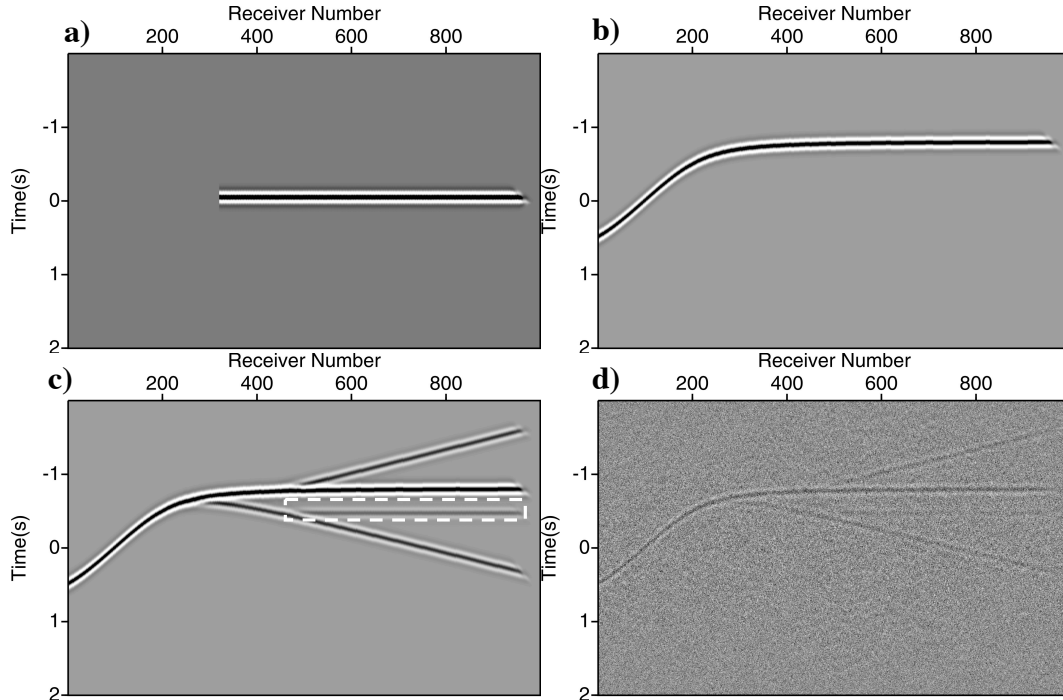

Figure 14. CPG gather for the four models in Figure 13. It is generated by correlating two different common receiver gathers in the time-space domain. (a) head wave. (b) reflection. (c) head wave plus reflection. Head wave contribution is denoted by a white box. (d) similar to (c), but with random noise.
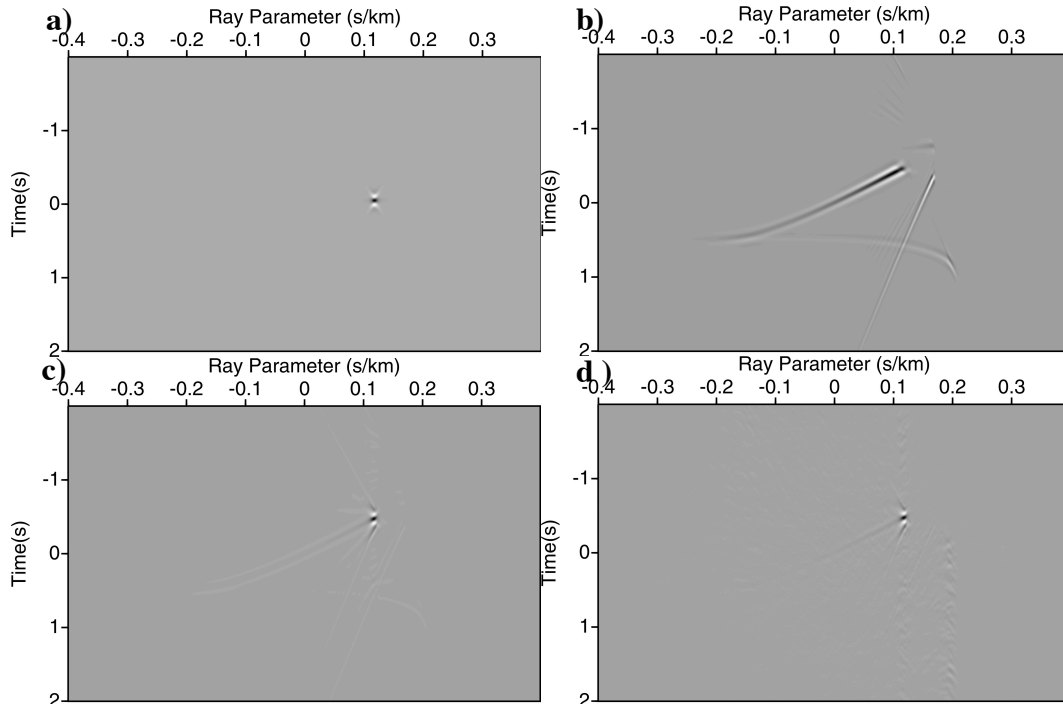

Figure 15. CPG gather generated with a plane-wave based approach. No filtering is applied. (a) head wave. (b) reflection. (c) head wave plus reflection. (d) similar to (c), but with random noise.

Figure 13 shows synthetic data containing head wave, reflection or both. In super-virtual interferometry, only head wave arrivals are treated as correlated useful information. While we want to avoid artifacts by windowing only head wave arrivals, for real problems, presence of other arrivals such as reflections and noise will result in spurious arrivals of the processed data. Thus, we generate synthetic data for four different scenarios; corresponding CPG gather using a time-space domain approach is shown in Figure 14. In comparison, CPG gather using a plane-wave based approach is shown in Figure 15.

For the pure head wave case (Figure 13a), the CPG gather shows a perfectly flat event with a time-space domain approach (Figure 14a) and a focused point with a plane-wave domain approach (Figure 15a), respectively. For pure reflection case in Figure 13b, the far-offset reflection in the CPG gather shows a nearly flat event (Figure 14b), which may be falsely identified as a refraction arrival. However, with a plane-wave domain approach, there is no focusing point for the reflection arrival (Figure 15b). For the case with both reflection and refraction (Figure 13c), with a time-space domain approach, the refraction event in the CPG gather (Figure 14c) is only in the white box area. Thus, it requires careful filtering and muting to get rid of reflection arrivals. In comparison, with a plane-wave domain approach, we could easily identify the focusing point in Figure 15c. Thus, we can easily suppress the influence of reflection arrivals. In addition, if we zoom in, we can see a flat event passing through the focusing point. Therefore, we can choose a range of ray parameters to stack the CPG gather. When the data is noisy (Figure 13d), with a time-space domain approach, refraction events in the CPG gather (Figure 14d) may be hard to identify because the amplitude is very small. In comparison, however, with a plane-wave domain approach, we can suppress the noise in the CPG gather (Figure 15d). This is because plane-wave transform involves stacking along ray parameters, which can attenuate the random noise.

We use our approach to one line of Ocean Bottom Seismometer (OBS) survey across Taiwan and the western Philippine Sea (McIntosh et al., 2005). The data was collected in four components (three component gimbaled 4.5 Hz geophones and a hydrophone). The seismic lines were shot with 100m spacing with a maximum of about 1500 shots. Initial data processing includes clock-drift correction, band-pass filtering and rotation of the horizontal component to radial and transverse components. Figure 16 shows a vertical geophone component of at one OBS station. The seismogram is plotted with a reduction velocity of 8.0 km/s, which flattens the Pn arrival. Another notable arrival at near offset is PSP arrival, which is partially converted as shear arrival. We think the P-wave mode of PSP arrival has likely converted into shear-mode before it arrives at the crust-mantle boundary. However, we cannot make a conclusive judgment because we don't know the shear-wave velocity strucure of this area. We can observe that shear-wave data are weaker and thus nosier than primary head waves. This is typical for most OBS surveys.

We then window the data around the PSP arrivals for every component in each OBS gather with a muting window of about 3.0 s. After that, we cross-correlate traces recorded at two different OBS stations for each component to generate CPG gather. A comparion of the radial horizontal component CPG gather obtained with a time-space domain approach and a plane-wave domain approach is shown in Figure 17. To increase the coherency, we use the super-

virtual gather at one location, which is suggested by Bharadwaj et al., (2011). CPG gather in the plane-wave domain shows a focusing refraction event at about 2.5 s and also a flat event because of imperfect focusing.
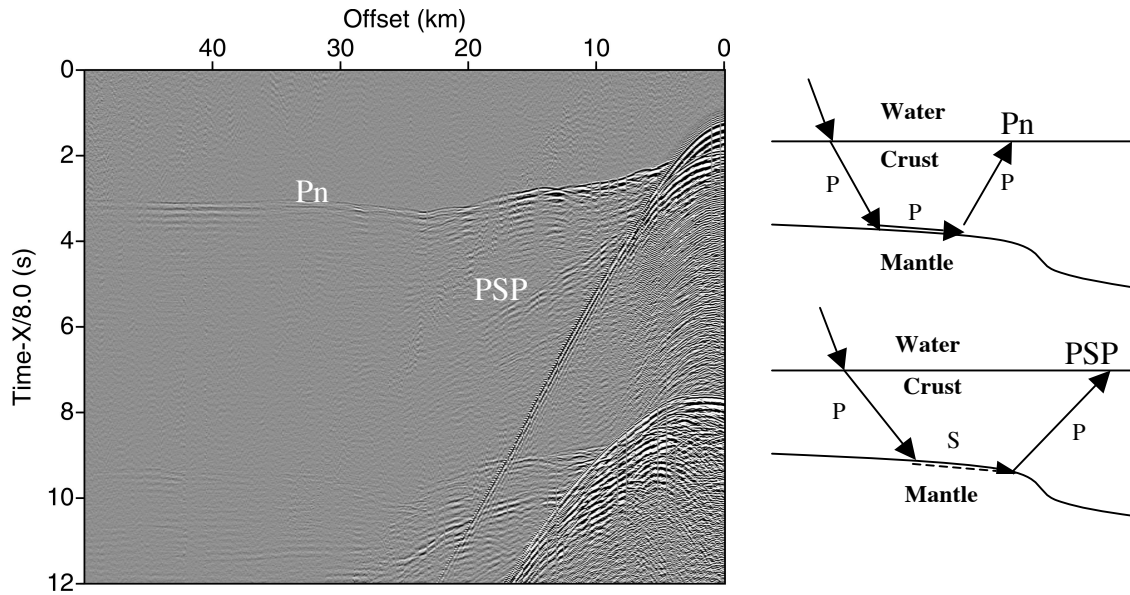

Figure 16. An example OBS data. Vertical component is shown. Two major refraction arrivals are Pn (refracted in the subducting slab) and PSP (refracted shear wave). Right diagram shows the ray-paths of the two different arrivals. The incident P-wave mode of PSP arrival in the crust has very likely been converted into shear-mode before it arrives at the crust-mantle boundary.
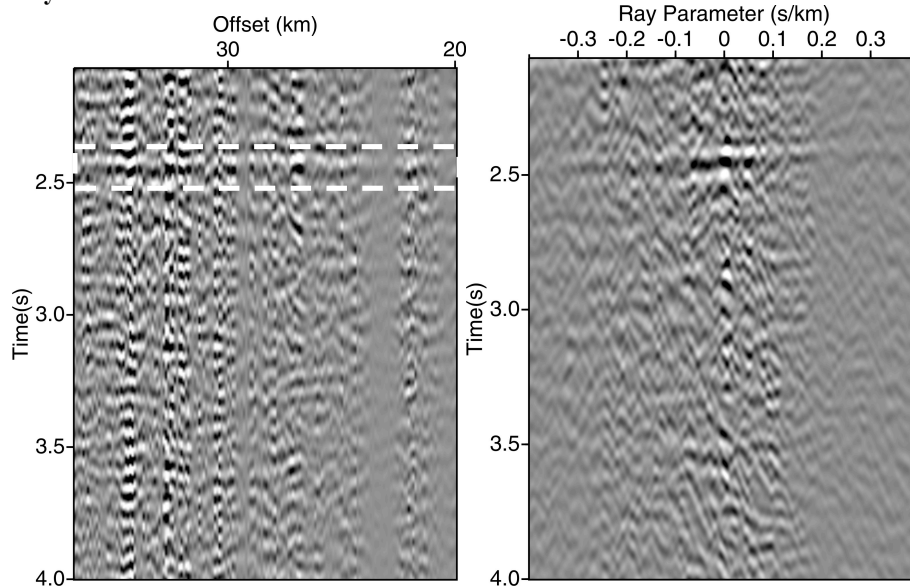

Figure 17. Comparison of the CPG gather obtained by correlating the radial horizontal component of the data at two stations. Super-virtual gather at one location is used to increase the coherency. Left: time-space domain approach. The flat event is marked in white box. Right: Plane-wave domain approach.

Figure 18 shows a comparion of the original data and processed data with super-virtual interferometry for vertical component and horizontal component. Because of the lack of refraction at far-offset for vertical component at every OBS station, super-virtual gather does not show much improvement of the far-offset refractions (Figure 18a and b). It shows even poorer result at near-offset because this technique focuses on the improvement of post-critical refractions. However, we could observe a significant improvement of the radial horizontal component. The refraction at far-offset (30km-50km) before processing is not clear, while in the super-virtual gather is clear to see.
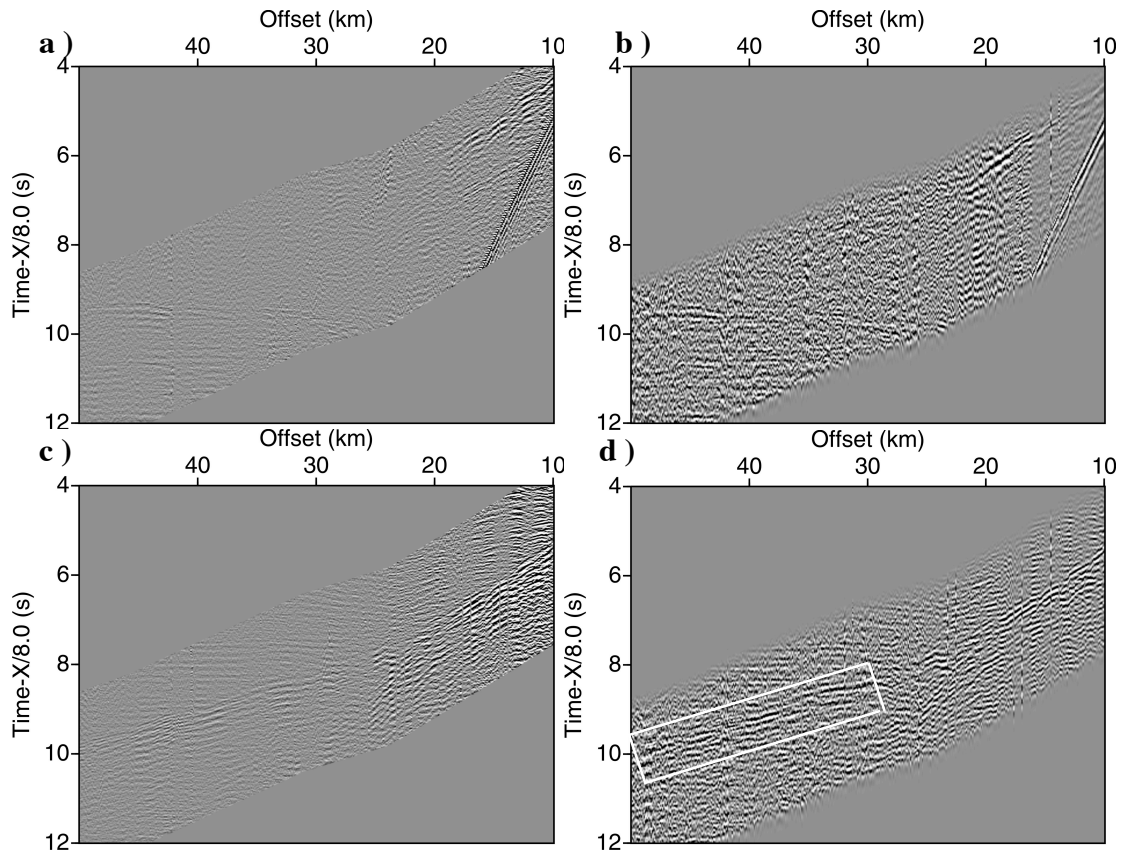

Figure 18. Comparison of the original data and processed data with super-virtual interferometry. (a) original vertical component. (b) super-virtual vertical component. (c) original horizontal (radial) component. (d) super-virtual horizontal (radial) component. While far-offset shear refracted wave of the vertical component does not show much improvement because the lack of far-offset signal at each OBS stations, the horizontal component shows significant far-offset enhancement. Far offset PSP arrival is contained in the white box area.

CONCLUSIONS

We present a new redatuming method in the plane-wave domain for controlled-source seismic interferometry. This method can be applied to any applications of controlled source interferometry if plane-wave transform is applicable to that data. Mathematically, it can be easily explained by the cancelation of waves that have common ray parameters. Using synthetic data generated with finite differences, we demonstrate that our method is effective in reconstructing

virtual seismic responses from SSP and VSP data. We also demonstrate the effectiveness of this method with synthetic refraction data and a real OBS data.

Compared with interferometry in the time-space domain, our method offers several advantages. It transforms irregularly acquired seismic data into a regular coordinate system. It can allow us to flexibly choose ray parameters so that we can selectively redatum the events we are mostly interested in and perform directional redatuming. A CPG gather generated with this approach for super-virtual study can help to reduce the effects of undesired phases and random noise. It also can reduce the computational cost if a large number of traces need to be crosscorrelated.

ACKNOWLEDGMENTS

REFERENCES

Vidal A. C., J. van der Neut, D. Draganov, G. G. Drijkoningen, and K. Wapenaar, 2011, Retrieval of reflections from ambient noise using the incident fields (point-spread function) as a diagnostic tool: 73th Conference and Exhibition, EAGE.

Bakulin A. and R. Calvert, 2006, The virtual source method: Theory and case study, Geophysics, Vol. 71, SI139-SI150.

Bharadwaj, P., G. T. Schuster, I. Mallison, and W. Dai, 2011, Theory of supervirtual refraction interferometry, Geophys. J. Int., doi: 10.1111/j.1365-246X.2011.05253.x.

Claerbout J. F., 1985, Imaging the earth's interior: Blackwell Science Inc.

Curtis, A., 2009, Source-receiver seismic interferometry: 79th Annual International

Meeting, SEG, ExpandedAbstracts, 3655–3658.

Draganov, D., K. Wapenaar, and J. Thorbecke, 2006, Seismic interferometry: Reconstructing the Earth's reflection response, Geophysics, 71, SI61– SI70.

Draganov, D., K.Wapenaar,W. Mulder, J. Singer, and A. Verdel, 2007, Retrieval of reflections from seismic background-noise measurements: Geophysical Research Letters, 34, L04305-1–L04305-4.

Dong, S., J. Sheng, and G. T. Schuster, 2006. Theory and practice of refraction interferometry, SEG Expanded Abstracts, 25, 3021–3025.

Foster, D. J., and C. C. Mosher, 1992, Suppression of multiple reflections using the Radon transform, Geophysics, 57, 386–395.

Liu, F.,M.K. Sen, and P. L. Stoffa, 2000, Dip selective 2-D multiple attenuation in the plane-wave domain: Geophysics, 65, 264–274.

Lu, R., M. E. Willis, X. Campman, J. Ajo-Franklin, and M. N. Toksöz, 2008, Redatuming through a salt canopy and target-oriented salt-flank imaging, Geophysics,Vol.73, S63–S71.

Mallinson, I., Bharadwaj, P., Schuster, G. & Jakubowicz, H., 2011. Enhanced refractor imaging by super-virtual interferometry, Leading Edge, 30, 546–550, doi:10.1190/1.3589113.

Mehta, K., Bakulin A., Sheiman J., Calvert R., and Snieder R., 2007, Improving the virtual source method by wavefield separation, Geophysics, Vol. 72, V79-V86.

McIntosh, K. D., Y. Nakamura, T.-K. Wang, R.-C. Shih, A. T. Chen, and C.-S. Liu, 2005, Crustal-scale seismic profiles across Taiwan and the western Philippine Sea, Tectonophysics, 401, 23-54.

Rickett, J., and J. Claerbout, 1999, Acoustic daylight imaging via spectral factorization: Helioseismology and reservoir monitoring: The Leading Edge, 18, 957–960.

Sabra, K., Gerstoft, P., Roux, P., Kuperman, W.A., Fehler, M.C., 2005, Extracting time- domain Green's function estimates from ambient seismic noise. Geophysical Research Letters 32 (3), 1–5.

Schuster, G. T., 2001, Theory of daylight/interferometric imaging: Tutorial: 63rd Annual Conference and Exhibition, EAGE, Extended Abstracts, A32-1-A32-4.

Schuster G.T. and M. Zhou, 2006, A theoretical overview of model-based and correlation-based redatuming methods, Geophysics, 71, SI103-SI110.

Schuster G.T. 2009. Seismic Interferometry: Cambridge University Press.

Sen. M. K., and A. Mukherjee, 2003, t-p analysis in transversely isotropic media, Geophysical Journal International: Vol. 154, 647-658.

Stoffa, P. L., ed., 1989, Tau-p: A plane wave approach to the analysis of seismic data: Kluwer Academic Publishers.

Stoffa, P. L., M. K. Sen, R. Seifoullaev, R. Pestana, and J. Fokemma, 2006, Plane-wave Depth migration, Geophysics, Vol. 75, S261-S272.

Tatham, R. H., 1989, Tau-p filtering, in P. L. Stoffa, ed., Tau-p: A plane wave approach to the analysis of seismic data: Kluwer Academic Publishers, 35–70.

Wapenaar, K., 2004, Retrieving the elastodynamic Green's function of an arbitrary inhomogeneous medium by cross correlation: Physical Review Letters, 93, 254301.1-254301.4.

Wapenaar K., 2006, Green's function retrieval by cross-correlation in case of one-sided illumination: Geophysical Research Letters, 33, L19304-1–L19304-6.

Wapenaar K., D. Draganov, R. Snieder, X. Campman, and A.Verdel, 2010 a, Tutorial on seismic interferometry: Part 1 - Basic principles and applications, Geophysics, Vol. 75, 195-209.

Wapenaar K., E. Slob, R. Snieder, and A. Curtis, 2010 b, Tutorial on seismic interferometry: Part 2 - Underlying theory and new advances, Geophysics, Vol. 75, 211-227.

Vigh D., and E. Starr, 2008, 3D prestack plane-wave, full waveform inversion, Geophysics, Vol.73, VE135–VE144.